THE JOURNAL OF BIOLOGICAL CHEMISTRY
Vol. 280, No. 18, Issue of May 6, pp. 18442–18451, 2005
Printed in U.S.A.

Reconstitution of Nup157 and Nup145N into the Nup84 Complex*[S]

Received for publication, November 11, 2004, and in revised form, January 28, 2005
Published, JBC Papers in Press, March 1, 2005, DOI 10.1074/jbc.M412787200

Malik Lutzmann‡, Ruth Kunze‡, Karin Stangl‡, Philipp Stelter‡, Katalin Fejes Tóth§, Bettina Böttcher¶, and Ed Hurt‡‖

From the ‡Biochemie-Zentrum der Universität Heidelberg, Im Neuenheimer Feld 328, 69120 Heidelberg, Germany, the ¶European Molecular Biology Laboratory, D-6900 Heidelberg, Germany, and the §Kirchhoff-Institut für Physik, Universität Heidelberg, 69120 Heidelberg, Germany

About 30 different nucleoporins (Nups) constitute the nuclear pore complex. We have affinity-purified 28 of these nuclear pore proteins and identified new nucleoporin interactions by this analysis. We found that Nup157 and Nup170, two members of the large structural Nups, and the Gly-Leu-Phe-Gly nucleoporin Nup145N specifically co-purified with members of the Nup84 complex. In addition, Nup145N co-enriched during Nup157 purification. By *in vitro* reconstitution, we demonstrate that Nup157 and Nup145N form a nucleoporin subcomplex. Moreover, we show that Nup157 and Nup145N bind to the heptameric Nup84 complex. This assembly thus represents approximately one-third of all nucleoporins. To characterize Nup157 structurally, we purified and analyzed it by electron microscopy. Nup157 is a hollow sphere that resembles a clamp or a gripping hand. Thus, we could reconstitute an interaction between a large structural Nup, an FG repeat Nup, and a major structural module of the nuclear pore complex.

Nucleocytoplasmic transport occurs through nuclear pore complexes (NPCs),[1] highly elaborate supramolecular assemblies within the double nuclear membrane (1, 2). The core structure of the NPC is formed by a spoke complex, which is sandwiched between a cytoplasmic and a nuclear ring. The eight spoke units, as part of the 8-fold symmetrical NPC array, surround the center of the NPC through which active nucleocytoplasmic transport is thought to take place. Moreover, a nuclear basket and short cytoplasmic fibrils, which are attached to the nuclear ring and the cytoplasmic ring of the NPC, respectively, can be visualized by high resolution electron microscopy (3–5).

About 30 different nucleoporins constitute the NPC in yeast and higher eukaryotes (6, 7). Nucleoporins exist in 8-, 16- and 32-fold copies per NPC and, thus, this ~50-MDa structure is assembled from a relatively low number of components (6). Nucleoporins are grouped into two major classes, one class with FG repeats that functions directly in nucleocytoplasmic transport by binding the soluble transport receptors (8, 9), and another class that is devoid of FG repeat sequences and is considered as representing the predominant structural constituents of the NPC. Moreover, a few of the structural nucleoporins should mediate integration in the double nuclear membrane or organize the repeat-containing nucleoporins to form the active transport channel (for review, see Refs. 2 and 10).

In past years, significant progress has been made in the biochemical analysis of the NPC composition and organization of individual nucleoporins within NPC subcomplexes (1, 2, 10). Moreover, immuno-electron microscopy has revealed the relative location of nucleoporins within the overall NPC framework. Thus, the first models have emerged from these studies that discuss how nucleoporins could perform their distinct roles in NPC structure and nucleocytoplasmic transport (11–13).

One of the best characterized subcomplexes of the NPC is the Nup84 complex in yeast (14–16). This assembly is composed of seven subunits and was shown to perform several essential roles, including functions in nuclear envelope organization, NPC biogenesis, and mRNA export. Because none of the members of the Nup84 complex contain FG repeat sequences, which bind to the shuttling transport receptors, it is intriguing how this complex can specifically affect the nuclear export of poly(A)$^+$ RNA. A vertebrate Nup107-Nup160 complex (17–19), which is homologous to the yeast Nup84 complex, was also shown to be essential for the postmitotic nuclear pore assembly (19–21).

Recently, we have reported that the Nup84 complex could be reconstituted *in vitro* from its recombinant seven subunits and exhibits a Y-shaped structure in the electron microscope, which is indistinguishable from the native complex (16). Thus, the Nup84 complex can self-assemble in a modular way from distinct smaller nucleoporin construction units. Motivated by these findings, we sought to extend the Nup84 complex further by searching for new interaction partners and successively assembling them *in vitro* into the pre-existing complex. A nucleoporin interaction analysis has been performed recently (22). Protein interactions that occur at individual FG Nups were sampled using immobilized nucleoporins and yeast extracts. This study showed that several FG Nups also captured the hexameric Nup84 complex.

Here, we conducted a proteomic approach to unravel additional nucleoporin interactions. We found that Nup157 and Nup145N are specifically associated with purified members of the Nup84 complex. In agreement with these findings, Nup157 and Nup145N could be reconstituted into the heptameric Nup84 complex. We examined purified Nup157 in the electron microscope and found that it has a characteristic clamp-like structure. Our data thus show the interaction of a large struc-

* The costs of publication of this article were defrayed in part by the payment of page charges. This article must therefore be hereby marked "*advertisement*" in accordance with 18 U.S.C. Section 1734 solely to indicate this fact.

[S] The on-line version of this article (available at www.jbc.org) contains supplemental Fig. 1 (growth analyses of yeast strains expressing TAP-tagged nucleoporins), Fig. 2 (peptide mass fingerprinting of newly identified protein interactions), and Fig. 3 (sedimentation equilibrium ultracentrifugation of Nup145N).

‖ Supported by Deutsche Forschungsgemeinschaft Grant SFB 638/B2 and a grant from Fonds der Chemischen Industrie and to whom correspondence should be addressed. Tel.: 49-6221-544173; Fax: 49-6221-544369; E-mail: cg5@ix.urz.uni-heidelberg.de.

[1] The abbreviations used are: NPC, nuclear pore complex; GST, glutathione *S*-transferase; MALDI-TOF, matrix-assisted laser desorption/ionization-time of flight; Nup, nucleoporin; ProtA, protein A; TAP, tandem affinity purification; TEV, tobacco etch virus.

tural Nup with the Nup84 complex, a key structural module of the NPC.

EXPERIMENTAL PROCEDURES

Microbiological Techniques and DNA Manipulations—Microbiological techniques (growth and transformation of *Escherichia coli* and yeast) and standard DNA manipulations (cloning, PCR amplification, and ligation) were performed as described previously (16, 23).

Insertion of Yeast Nucleoporin Genes into E. coli Expression Vectors and Yeast 2μ Plasmids and Genomic Integration of the Tandem Affinity Purification (TAP) Tag—For expression in *E. coli*, the open reading frames of *Nup145N* and *Nup157* were amplified by PCR and cloned into pPROEXHT-GST-TEV (16). For bicistronic expression of GST-*Nup157* and GST-*Nup120*, the open reading frame of *Nup120* was amplified with a 5′ second ribosomal binding site and cloned downstream of the *Nup157* (16). Bicistronic expression of GST-*Nup84* and GST-*Nup157* was performed in a similar way. For overexpression in yeast, the open reading frames of *NUP157* and *NUP188* were cloned into the pNOPPATA2L 2μ plasmid (24) and transformed into yeast strains genomically disrupted for the gene of interest. For TAP tagging of the yeast nucleoporins, the cassette harboring the TAP tag was genomically integrated at the 3′-end of the genes as described (25).

Overexpression of Proteins in E. coli and Yeast—All recombinant protein expression in *E. coli* was done with the BL21 codon plus RIL strain (Stratagene) and performed as described previously (16), except that bicistronic expression of GST-*Nup157*/GST-*Nup120* was performed overnight at 16 °C and induced with 0.1 mM isopropyl-1-thio-β-D-galactopyranoside. Yeast cells overexpressing ProtA-tagged Nups were grown in 2–6 liters of SDC-Leu medium at 30 °C to an OD of ~3.5. After pelleting the cells by centrifugation, the pellet was washed in cold water and NB buffer (150 mM NaCl, 50 mM KOAc, 20 mM Tris, pH 7.5, 2 mM $Mg(OAc)_2$, and 0.15% Nonidet P-40). The cell pellet was frozen in liquid nitrogen and stored at −20 °C.

Affinity Purification of Chromosomally TAP-tagged Yeast Nucleoporins and Mass Spectrometry Analysis—Affinity purification of nucleoporins from 2–6 liters of yeast cultures grown at 30 °C in YPD (1% yeast extract, 2% peptone, and 2% dextrose) medium to an OD of ~3.5 was performed as described (26). Only the first affinity purification step of the TAP method (TEV elution) was applied. The second step (*i.e.* calmodulin-Sepharose) was omitted, because it was found to be disruptive for some nucleoporin interactions (*e.g.* Nup133 dissociated from the Nup84 complex upon incubation with calmodulin-Sepharose.[2] Affinity purification of Nup53 and Nup59 were not successful. TEV-eluted nucleoporins were analyzed on Novex SDS 4–12% gradient polyacrylamide gels (Invitrogen) and stained with colloidal or normal Coomassie R250 (both from Sigma). Mass spectrometry using tryptic digests of bands excised from a Coomassie-stained SDS-polyacrylamide gel was performed according to (27). Analysis was performed on a Bruker Reflex III MALDI-TOF instrument. Identification of protein bands was achieved by peptide mass fingerprints using Mascot (Matrix Science) and the MSDB mass spectrometry protein data base.

Affinity Purification of GST- and ProtA-tagged Proteins—Purification of GST-tagged proteins from *E. coli* was performed in NB buffer containing 10% glycerol as described (16). Overexpressed ProtA-tagged Nup157 and Nup188 were affinity-purified in NB buffer, which was supplemented with 0.15% Nonidet P-40 and a mixture of protease inhibitors during cell lysis. After cell breakage and centrifugation, the soluble fraction was incubated with 0.5 ml of IgG-Sepharose (Amersham Biosciences) per 2 liters of culture, and beads were washed with 30 volumes of NB buffer plus 0.5 mM dithiothreitol. TEV cleavage was performed for 2 h at 16 °C in 150 μl of Luria-Bertani medium with 0.5 mM dithiothreitol and 10 μl of TEV protease (1 mg/ml). Ion exchange (Mono Q HR5/5; Amersham Biosciences) and gel filtration chromatography (Superose 6 HR10/30 and Superdex 200 HR10/30; Amersham Biosciences) were performed on an ÄKTA basic system (Amersham Biosciences). All gel filtration chromatography and binding assays of Nup145N, Nup157, and the Nup84 complex were performed in NB buffer. The heptameric Nup84 complex was reconstituted as described (16).

Electron Microscopy and Image Processing—For negative staining, 5 μl of sample were placed on a freshly glow-discharged, carbon-coated grid and then washed four times with water, stained with uranyl formate (2% w/v), and dried. Electron microscopy was carried out on a Philips CM120 BioTwin electron microscope equipped with a tungsten filament operating at 100 kV. Micrographs of selected areas were recorded with a wide angle charge-coupled device camera (DV300W1; Gatan) at a nominal magnification of 93,000.

For image processing, micrographs of Nup157 were taken at a calibrated magnification of 50,000 and scanned with the Zeiss Scai Scanner at a step size of 21 μm/pixel, which corresponded to 4.2 Å at specimen level. 5,000-particle images were selected and boxed using the MRC image-processing package (28). Boxed particle images were imported to the IMAGIC 5 package (29), which was used for all further steps. Particles were normalized and band pass-filtered with a low frequency cutoff of 1/170 $Å^{-1}$ and a high frequency cutoff of 1/9 $Å^{-1}$. The box size of the extracted particle images was 50 × 50 pixels. For initial alignment the alignment by classification strategy was chosen. After a few rounds of refinement the class averages stabilized. Relative spatial orientations of the class averages were determined by sinogram correlation. This process was started several times, beginning with different class averages for the initial determination of Euler angles. Three-dimensional maps were calculated using the exact weighted back projection algorithm. Determination of Euler angles and calculation of three-dimensional maps were repeated until the map converged into a stable shape from which projections could be generated that were similar to all of the initially observed class averages. A three-dimensional map was further refined by projection matching. This process was repeated several times. Resolution of the final map was estimated by Fourier shell correlation (FSC). The FSC was 0.5 at a spatial frequency of 1/17.5 $Å^{-1}$ and crossed the 3 σ curve at 1/14 $Å^{-1}$.

Analytical Ultracentrifugation—Analytical sedimentation equilibrium ultracentrifugation was carried out at 4 °C on a Beckman Optima XL-A analytical ultracentrifuge equipped with absorbance optics and an An60 Ti rotor. From the amino acid sequence of Nup145N, a molecular mass of 64.8 kDa, an extinction coefficient at 280 nm of $\epsilon = 3.14 \cdot 10^4$ $M^{-1} \cdot cm^{-1}$, and a partial specific volume of $\bar{\nu} = 0.7114$ $ml \cdot g^{-1}$ at 4 °C were calculated from the amino acid composition with the program SEDNTERP version 1.08.[3] Nup145N was analyzed in a buffer containing 150 mM NaCl, 50 mM potassium acetate, 20 mM Tris-HCl, pH 7.5, and 2 mM magnesium acetate with a density of $\rho = 1.0093$ $g \cdot ml^{-1}$ as calculated with SEDNTERP. Sedimentation equilibrium ultracentrifugation runs were performed with protein concentrations of 1.6, 3.2, and 7.4 μM and at angular velocities of 7,000 and 10,000 rpm. Equilibrium was obtained after 24 h. Absorbance data were collected at 280 and 230 nm by averaging 10 scans with radial increments of 0.001 cm in step mode. The molecular mass of Nup145N was determined by global fitting of the data to an ideal single component model with the software UltraScan version 6.2 (www.ultrascan.uthscsa.edu).

RESULTS

Proteomic Analysis of Nucleoporin Interactions—To obtain a more comprehensive picture of nucleoporin interactions in the NPC, we sought to affinity-purify all yeast Nups in a comparative way and identify stoichiometrically and sub-stoichiometrically co-purifying bands. Therefore, *NUP* genes were chromosomally tagged with the TAP construct (26). Functionality of the TAP-tagged nucleoporins, which are essential for cell growth or whose deletion causes a slow growth phenotype, was tested by growth analysis (supplemental Fig. 1*A*, available in the on-line version of this article). In the case of non-essential Nups whose deletion does not cause a growth inhibition, growth analyses did not reveal whether the TAP tag impairs nucleoporin function; however, all of these yeast Nups had already been tagged at the carboxyl terminus by ProtA or a green fluorescent protein and were shown to be assembled into the NPCs (6, 30).

Subsequently, TAP-modified nucleoporins were affinity-purified from whole cell lysates under standardized conditions (see "Experimental Procedures"). We applied only the first affinity purification step of the TAP method (*i.e.* proteolysis-mediated elution from IgG-Sepharose by the TEV protease) but omitted the second step (*i.e.* calmodulin-Sepharose), which was found to be disruptive for some known nucleoporin interactions.[2] The TEV eluates from the various nucleoporin purifications were analyzed by SDS-PAGE, and distinct bands discern-

[2] R. Kunze and M. Lutzmann, unpublished results.

[3] Developed by J. Philo, D. Hayes, and T. Laue; www.jphilo.mailway.com/download.htm.

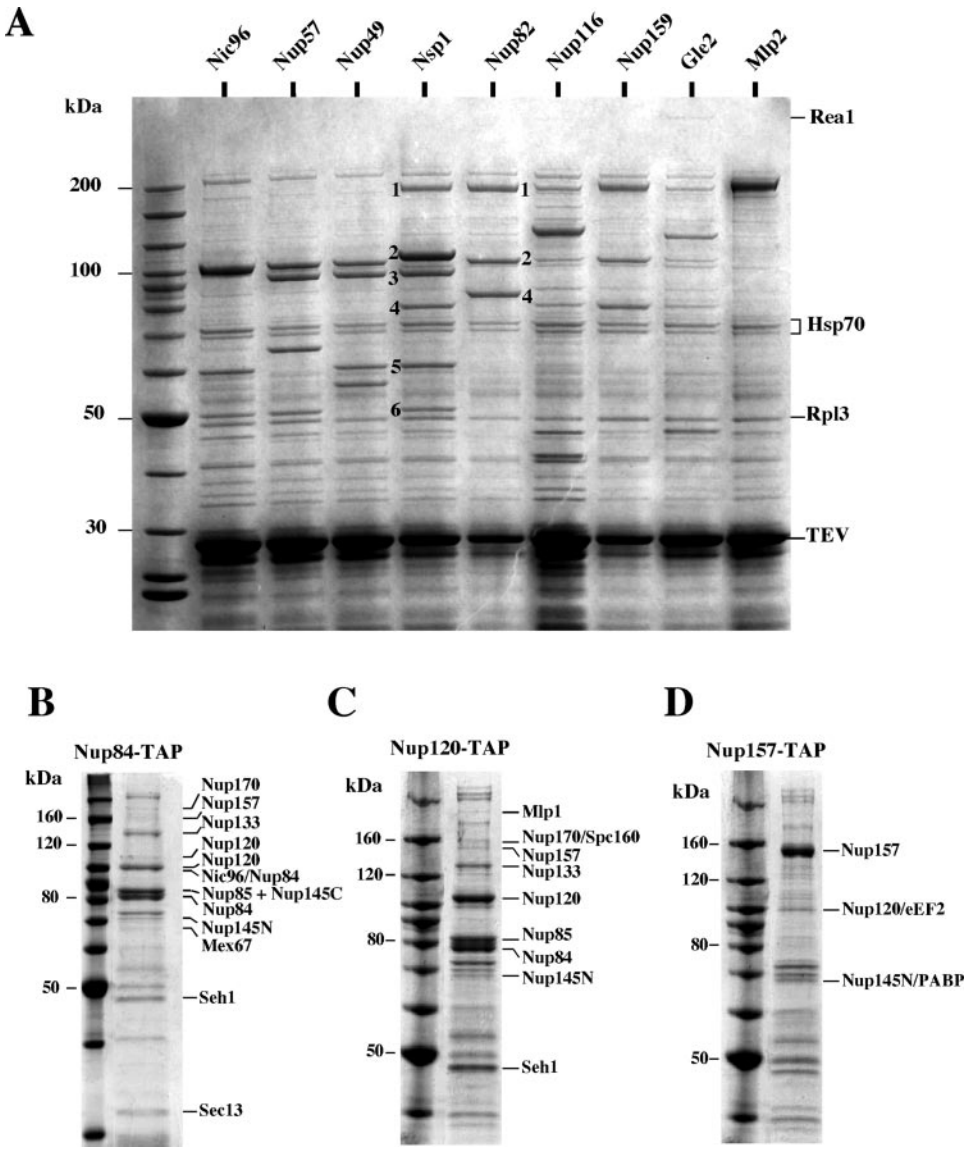

FIG. 1. ***In vivo* interactions between yeast nucleoporins.** *A*, affinity purification of the indicated TAP-tagged Nups by IgG-Sepharose and TEV elution followed by SDS-PAGE and Coomassie staining. For Nsp1 and Nup82 purifications, the co-purifying nucleoporins are indicated in the columns as follows: *band(s) 1*, Nup159; *band(s) 2*, Nsp1; *band 3*, Nic96; *band(s) 4*, Nup82; *band 5*, Nup57; and *band 6*, Nup49. Note that the calmodulin binding tag present on the bait protein increases the molecular mass by ~5 kDa. Protein bands were identified by mass spectrometry (see Table I). Marked on the right are prominent contaminants (*e.g.* Hsp70 and Rpl3) and the TEV protease. Interestingly, Rea1 was detected in the Gle2 and Nup116 preparations. *B–D*, affinity purification of Nup84-TAP (*B*), Nup120-TAP (*C*), and Nup157-TAP (*D*). Only the nucleoporin bands identified by mass spectrometry, but not contaminants, are labeled on the *right*. Shown are also molecular mass markers.

ible by Coomassie staining were excised and analyzed by MALDI-TOF mass spectrometry (see "Experimental Procedures" and supplemental Fig. 2, available in the on-line version of this article). Because of the omission of the second affinity purification step, all of the nucleoporin purifications were contaminated by common impurities (*e.g.* heat shock proteins, fatty acid synthetase, translation factors, ribosomal proteins, etc.) that tend to stick to IgG-Sepharose. Nevertheless, side-by-side comparison of the different nucleoporin preparations allowed us to identify specific co-purifying bands (Fig. 1). This comprehensive analysis confirmed many of the known nucleoporin interactions and convincingly revealed the three major structural modules of the NPC, namely the Nic96 complex (Nsp1-Nup57-Nup49-Nic96), the Nup82 complex (Nup82-Nsp1-Nup159-Nup116-Gle2), and the Nup84 complex (Nup84-Nup85-Nup120-Nup133-Nup145C-Seh1-Sec13) (Fig. 1 and Table I) (for cross references, see Refs. 1 and 2).

Nup170, Nup157, and Nup145N Associate in Vivo with the Nup84 Complex—Importantly, our systematic nucleoporin purifications revealed several new interactions. Thus, we found Sac3 in the Nup60 preparation (Table I and supplemental Fig. 2). These data are consistent with previous observations that the pore-associated mRNA export factor Sac3 interacts functionally with Nup60 and Nup1 (31). Moreover, we could detect Kap123 in the Nic96 preparation along with low amounts of the Rea1 AAA^+-type ATPase, which is associated with nucleoplasmic pre-60 S ribosomal subunits (32), in the TAP-purified Gle2 and Nup116 purifications (Fig. 1, Table I, and supplemental Fig. 2).

Additionally, several members of the Nup84 complex co-enriched a specific set of nucleoporins not previously known to interact. Affinity-purified Nup84, Nup120, and Nup145C all contained sub-stoichiometric amounts of Nup170, Nup157, and Nup145N (Fig. 1, *B* and *C*, Table I, and supplemental Fig. 2). In addition, we found Nic96 and Mex67 in the Nup84 preparation and Mlp1 in the Nup120 purification (supplemental Fig. 2). It was recently suggested that Mlp1 is bound via Nup60 and Nup145 to the NPC (33) and that the mRNA export receptor

TABLE I

Proteomic analysis of yeast nucleoporin interactions

TAP-tagged proteins are indicated in the top row (Bait). Co-purifying proteins identified by mass spectrometry are listed in the far left column (Found) and indicated by shaded (medium and dark gray) rectangles in the column below the name of each bait protein. Previously known nucleoporin interactions found in this study are denoted by dark gray rectangles. Signified by light gray rectangles are the bait proteins, which were also identified by mass spectrometry.

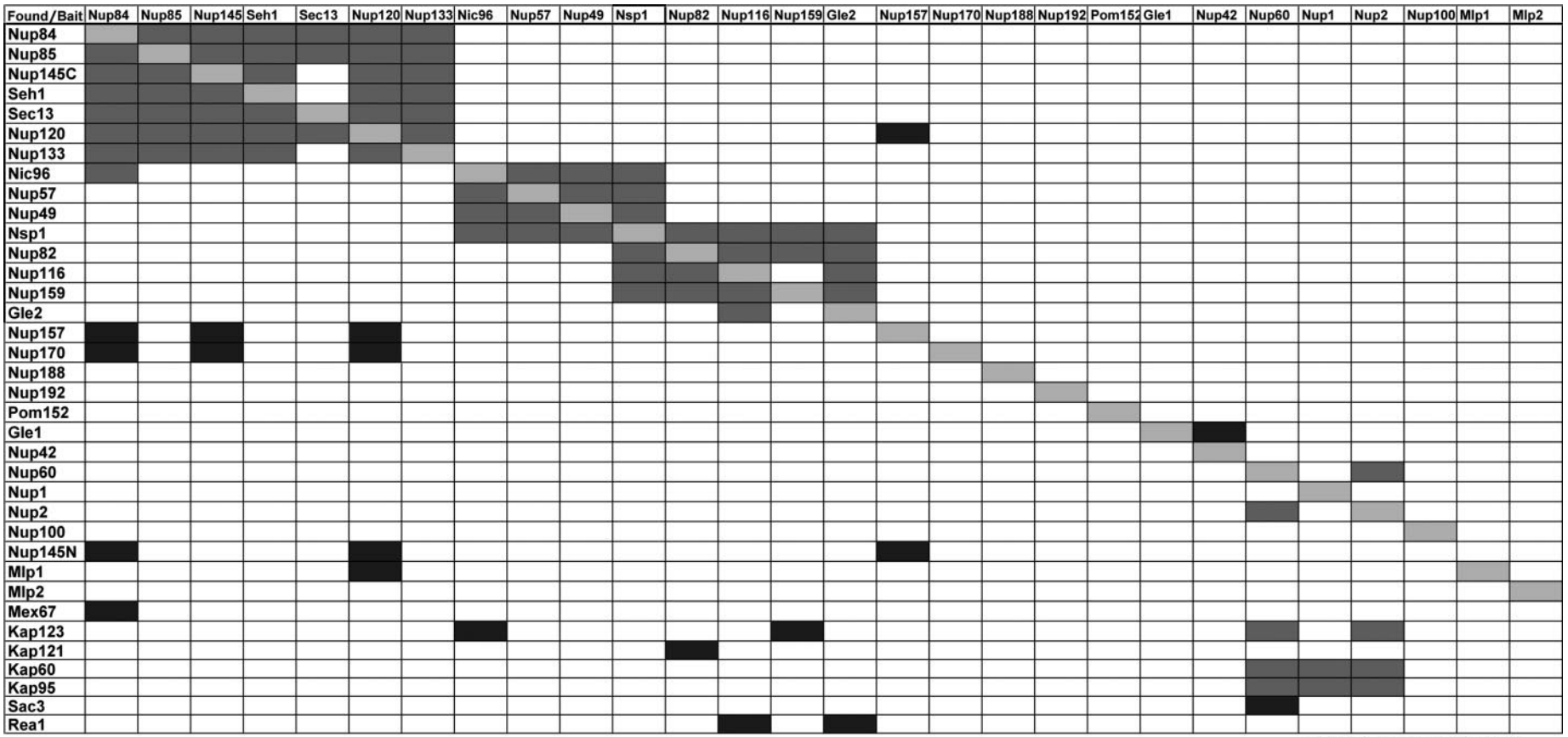

Table_1 (Lutzmann et al., 2005)

Mex67 interacts with Nup85 (23). Moreover, Nup98 (the vertebrate counterpart of Nup145N) was described to interact with the Nup107-Nup160 complex (the vertebrate counterpart of the Nup84 complex; Refs. 18 and 34). Further biochemical analysis and *in vitro* reconstitution are required to show that these observed protein interactions are direct.

Consistent with the findings described above, affinity-purified Nup157 also revealed the presence of Nup120 and Nup145N (Fig. 1*D*). It is not clear why only Nup120 but not the other members of the Nup84 complex was found in the Nup157 preparation (see "Discussion"). Moreover, we could not detect members of the Nup84 complex in the Nup170 preparation (Table I). This may not be significant, as Nup170-TAP could not be affinity-purified in satisfactory levels.[4] Altogether, the data suggested that Nup170, Nup157, and Nup145N could be in physical contact with the Nup84 complex.

In Vitro Reconstitution of the Nup157-Nup145N Heterodimer—To further study the interactions of Nup157 and Nup145N with the Nup84 complex, we performed *in vitro* reconstitution. First, we analyzed whether Nup157 and Nup145N can directly bind to each other. To perform this experiment, GST-tagged Nup145N was expressed in *E. coli* and purified to homogeneity by GST-affinity purification, TEV cleavage, and gel filtration chromatography. Nup145N, which has a calculated M_r of ~65,000, eluted from the gel filtration column in a relatively sharp peak with an apparent M_r of ~200,000 (Fig. 2*A*).

Analytical ultracentrifugation was conducted to analyze the association state of Nup145N in greater detail (supplemental Fig. 3, available in the on-line version of this article). The apparent molecular mass of Nup145N was determined to be 61.4 kDa from a fit to a single component model. No systematic deviations could be detected as evident from inspection of the residuals in supplemental Fig. 3. This demonstrates that the model describes the data accurately and that only one component was present. The molecular mass of Nup145N calculated from its primary sequence is 64.8 kDa, which comes close to the value determined by analytical ultracentrifugation. Thus, Nup145N exists as a monomer under physiological buffer conditions and the protein concentrations used. We assume that the unusual elution of purified Nup145N from the gel filtration column is due to the presence of GLFG repeats. It was recently reported that FG repeat domains within nucleoporins are natively unstructured and induce atypical elution during gel filtration (35).

In contrast to Nup145N, expression of Nup157 in *E. coli* yielded mostly insoluble protein (data not shown). Therefore, we sought to exploit yeast as an expression system and overexpressed ProtA-tagged Nup157 from a high copy number (2 μ) plasmid. The protein was affinity-purified on IgG-Sepharose and eluted by TEV protease cleavage. The eluate was then applied to a gel filtration column yielding highly purified Nup157 that eluted at ~200 kDa (Fig. 2*B*).

To analyze whether purified Nup145N and Nup157 proteins can form a complex *in vitro*, GST-Nup145N immobilized on GSH beads was incubated with purified Nup157 from yeast. As shown in Fig. 2*C*, Nup157 bound to Nup145N in a ~1:1 stoichiometric ratio, as judged from the intensity of the Coomassie-stained bands. To show the specificity of this interaction, we tested whether Nup157 binds to GST alone. Only trace amounts of Nup157 were bound to GST beads (Fig. 2*C*). Moreover, we tested whether another large nucleoporin, Nup188, can interact with Nup145N *in vitro*. Similar to Nup157, ProtA-tagged Nup188 was expressed in yeast from a 2μ plasmid and purified by IgG-Sepharose and gel filtration chromatography. However, only very small amounts of Nup188 were seen to bind to GST-Nup145N (Fig. 2*C*).

To further characterize complex formation between Nup145N and Nup157, we mixed partially purified Nup145N and Nup157 in solution and monitored heterodimerization by gel filtration chromatography. The reconstituted Nup157-Nup145N complex eluted at ~400 kDa, which is two fractions earlier than the single subunits (compare Fig. 2*D* with *panels A* and *B*). Thus, Nup157 and Nup145N constitute a novel nucleoporin subcomplex.

In Vitro Reconstitution of Nup157 and Nup145N into the Nup84 Complex—Our next aim was to assemble the Nup157-Nup145N heterodimer into the heptameric Nup84 complex. For these reconstitution studies, the pre-assembled Nup84 complex, which consists of seven subunits (Nup84, Nup85, Nup120, Nup133, Nup145C, Seh1, and Sec13), was immobilized on GSH-Sepharose via the GST-tagged Nup145C subunit (see Ref. 16). Then, highly purified Nup157 from yeast (see Fig. 2*B*) and Nup145N purified from *E. coli* (see Fig. 2*A*) were incubated with the immobilized Nup84 complex. After a washing step to remove unbound material, proteins were eluted and analyzed by SDS-PAGE and Coomassie staining. As shown in Fig. 3*A*, Nup157 and Nup145N bound in a ~1:1 stoichiometry to the Nup84 complex, yielding an assembly of nine subunits with a calculated molecular mass of 820 kDa. However, when this supercomplex was subjected to gel filtration chromatography, most of it dissociated into the separate subcomplexes (data not shown). This suggests that the interaction between the Nup157-Nup145N heterodimer and Nup84 complex is not very strong. These *in vitro* findings are consistent with the observation that only small amounts of Nup157 and Nup145N were co-enriched during Nup84 complex purification from yeast lysates (see Fig. 1, *B–D*). In further reconstitution studies we showed that Nup157 (Fig. 3*B*) or Nup145N alone (data not shown) can bind to the pre-assembled Nup84 complex. This suggests that both Nup157 and Nup145N have separate binding sites on the Nup84 complex.

Interaction of Nup157 with Nup120-containing Subcomplexes—Our proteomic analysis showed that affinity-purified Nup157 contained Nup120, which is a member of the Nup84 complex (see Fig. 1*D*). Hence, we wanted to analyze whether Nup157 and Nup120 interact directly. To this end, GST-tagged Nup157 and untagged Nup120 were co-expressed from a bicistronic construct in *E. coli*. Significantly, Nup120 (identified by mass spectrometry) co-enriched with affinity-purified GST-Nup157 (Fig. 3*C*). However, *E. coli* heat shock proteins were also bound to beads, which could mean that Nup157 and/or Nup120 are not completely folded or that they expose hydrophobic binding sites. In contrast, bicistronic co-expression of another GST-tagged Nup (GST-Nup84), together with Nup157 in *E. coli*, did not reveal any co-enrichment of Nup157 during GST-Nup84 affinity purification (Fig. 3*C*). This suggests that Nup157 *per se* is not a sticky protein.

To obtain further evidence for a Nup157-Nup120 interaction, we tested the binding of soluble Nup157 purified from yeast to different *in vitro* reconstituted subcomplexes of the Nup84 complex immobilized on GSH-Sepharose (see Ref. 16). These analyses revealed that Nup157 was bound to the pentameric Nup120-Nup85-Seh1-Nup145C-Sec13 complex and the trimeric Nup120-Nup85-Seh1 complex (Fig. 3*D*). Importantly, Nup157 did not bind to complexes that lack Nup120 (*e.g.* the Nup85-Seh1, Nup145C-Sec13, and Nup133-Nup84 complexes). We conclude from these studies that Nup120 exhibits a binding site for Nup157 within the Nup84 complex.

Electron Microscopic Analysis of Purified Nup157—Because Nup157 and Nup145N could be efficiently purified and ob-

[4] K. Stangl, unpublished data.

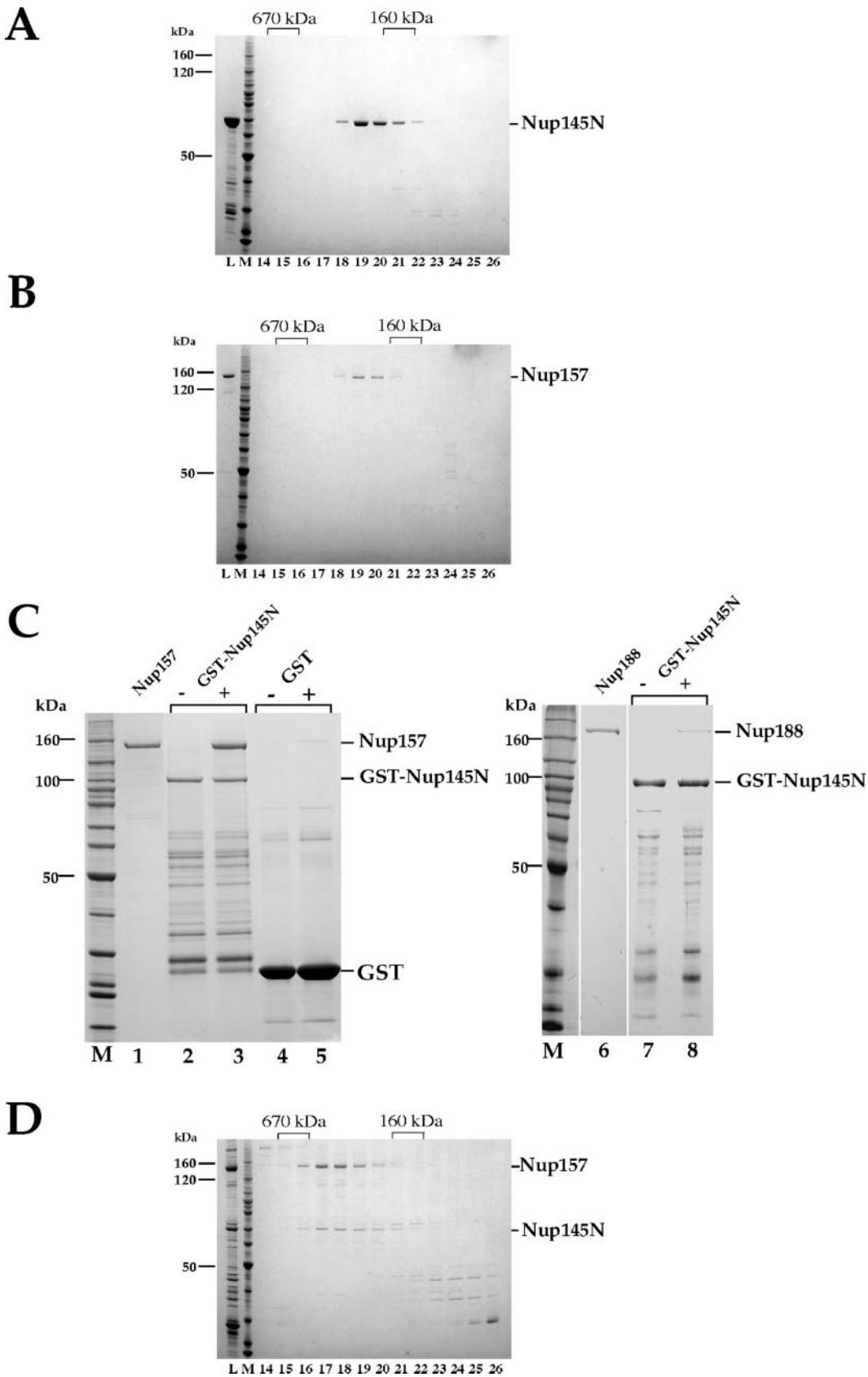

FIG. 2. **Nup157 and Nup145N form a heterodimer.** *A* and *B*, gel filtration of Nup145N purified from *E. coli* (*A*) and Nup157 purified from yeast (*B*) on a Superdex 200 HR column. Shown are the loaded proteins (*L*), a protein standard (*M*), and fractions 14–26. The column was calibrated with molecular mass markers (Bio-Rad) of 670, 158, 44, and 17 kDa (indicated on the *top*). *C*, *in vitro* binding of Nup157 to immobilized GST-Nup145N and GST. *Lane 1*, purified Nup157; *lane 2*, GST-Nup145 incubated with buffer; *lane 3*, GST-Nup145 incubated with purified Nup157; *lane 4*, GST incubated with buffer; *lane 5*, GST incubated with purified Nup157; *lane 6*, purified Nup188; *lane 7*, GST-Nup145 incubated with buffer; *lane 8*, GST-Nup145 incubated with purified Nup188; *M*, protein standard. *D*, gel filtration of the Nup157-Nup145N complex on Superdex 200 HR. Shown are the loaded proteins (*L*), a protein standard (*M*), and *fractions 14–26*. Indicated on the *right* are the positions of Nup157 and Nup145N.

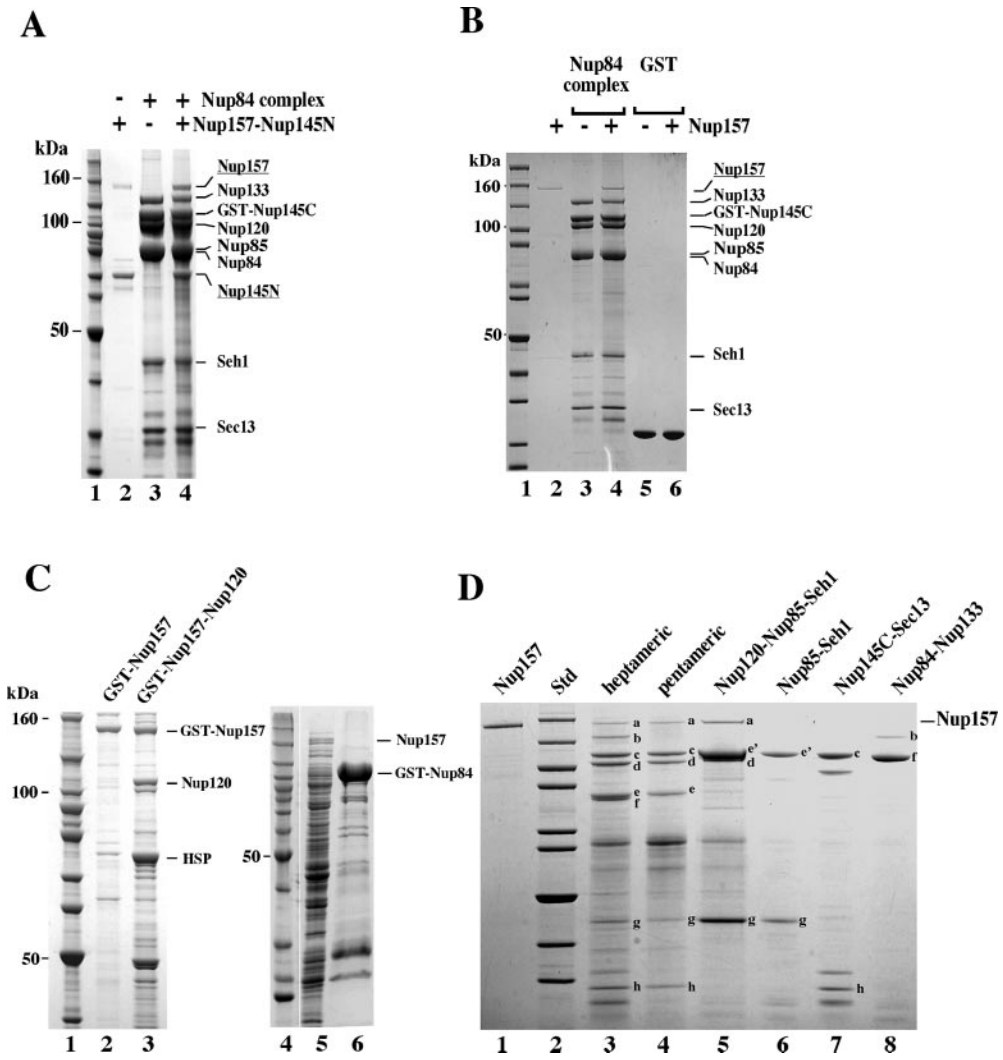

FIG. 3. **Reconstitution of a nine-subunit assembly between Nup157-Nup145N and the Nup84 complex.** *A*, *In vitro* binding of purified Nup157 and Nup145N to the reconstituted Nup84 complex. Purified and mixed Nup157 and Nup145N (*lane 2*) were incubated with the heptameric Nup84 complex immobilized on GSH beads via GST-Nup145C (*lane 4*). A molecular mass marker (*lane 1*) and buffer control (*lane 3*) are also shown. Bound proteins were analyzed by SDS-PAGE and Coomassie staining. *B*, *in vitro* binding of Nup157 to the reconstituted Nup84 complex. Purified Nup157 (*lane 2*) was incubated with the immobilized Nup84 complex (*lane 4*) or GST (*lane 6*). Buffer controls (*lanes 3* and *5*) are also shown. Bound proteins were analyzed by SDS-PAGE and Coomassie staining. Indicated on the *right* are the positions of the Nup proteins. *C*, Nup157 and Nup120 bind directly to each other. Molecular mass markers (*lanes 1* and *4*), GST-Nup157 (*lane 2*), GST-Nup157 co-expressed with Nup120 (*lane 3*), and GST-Nup84 co-expressed with Nup157 (*lane 6*) were purified from *E. coli* and TEV eluates analyzed by SDS-PAGE and Coomassie staining. *Lane 5* shows the *E. coli* lysate containing GST-Nup84 and Nup157. *D*, binding of soluble Nup157 purified from yeast to different *in vitro* reconstituted subcomplexes. Purified Nup157 (*lane 1*) was incubated with the immobilized complexes heptameric Nup84-Nup85-Nup120-Nup133-Nup145C-Seh1-Sec13 (*lane 3*), pentameric Nup85-Nup120-Nup145C-Seh1-Sec13 (*lane 4*), trimeric Nup85-Nup120-Seh1 (*lane 5*), dimeric Nup85-Seh1 (*lane 6*), dimeric Nup145C-Sec13 (*lane 7*), and dimeric Nup84-Nup133 (*lane 8*). Bound proteins were analyzed by SDS-PAGE and Coomassie staining. Bands were labeled as follows: *a*, Nup157; *b*, Nup133; *c*, GST-Nup145C; *d*, Nup120; *e*, Nup85; *e'*, GST-Nup85; *f*, Nup84; *g*, Seh1; and *h*, Sec13.

tained in pure form, we sought to study their morphology by transmission electron microscopy. For the purified Nup145N we could not see a discernible structure in the electron microscope.[5] This is most likely due to the small size of the Nup145N molecule and the presence of GLFG repeats, which are not structured and thus may not be contrasted enough by negative staining.

For negative staining of Nup157, we used fractions of the final gel filtration column that contained essentially pure protein (Fig. 4*A*). In the electron microscope, Nup157 showed a globular morphology with a diameter of ~12 nm. A significant number of Nup157 molecules exhibited an indentation (Fig. 4*A*). To find out whether the structure of overexpressed Nup157 differs from endogenous Nup157, we affinity-purified Nup157 from yeast that expressed chromosomally TAP-tagged *NUP157*. However, authentic Nup157 was indistinguishable from overproduced Nup157 (Fig. 4*A*).

Because micrographs of negatively stained Nup157 showed a homogeneous spread of particles, we could perform image processing to reveal more details of the Nup157 structure. By calculating the three-dimensional map of the protein, it became apparent that Nup157 was hollow and looked like a clamp or a gripping hand (Fig. 4*B*; see also "Discussion"). The outer dimensions of the clamp were 12 nm in the long direction and ~7–8 nm in the shorter direction.

DISCUSSION

From the ~30 yeast nucleoporins, about two-thirds are organized in biochemically stable NPC subcomplexes. However, the direct interacting partners for the remaining Nups are still unidentified (for review, see Refs. 2, 10, and 36). Moreover, it is not known how the stable NPC subcomplexes interact with

[5] M. Lutzmann, unpublished results.

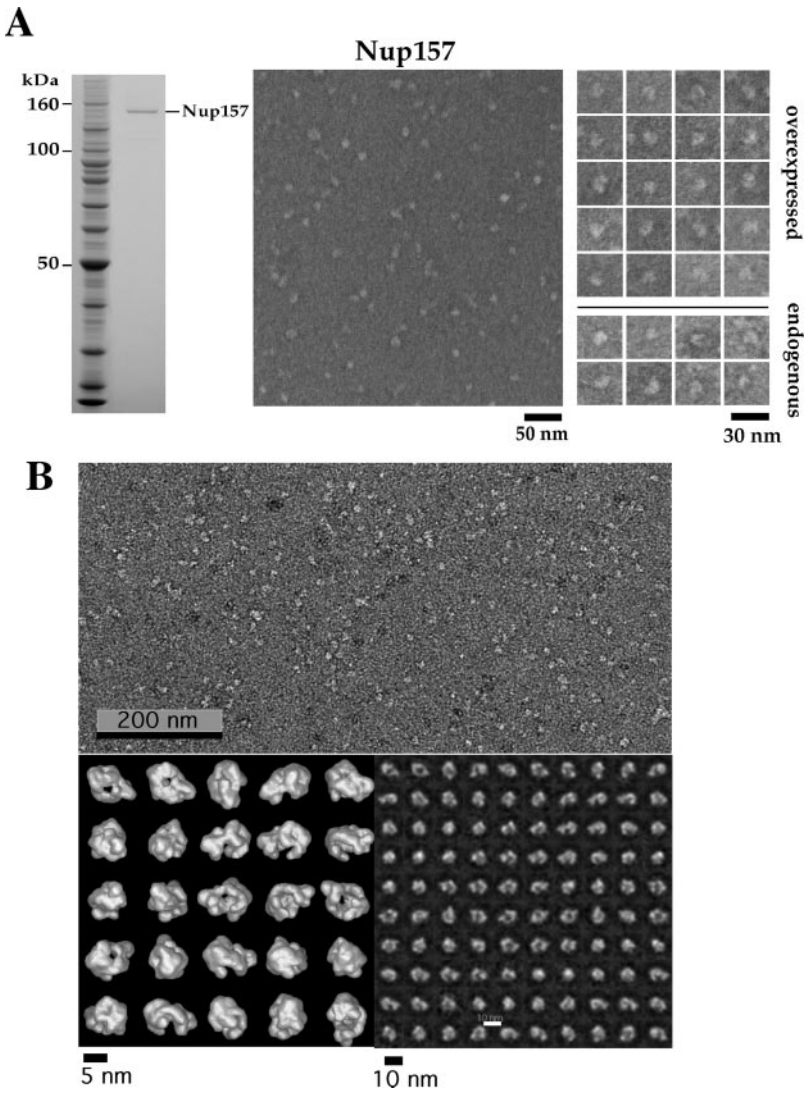

FIG. 4. **Electron microscopic analysis of purified Nup157.** *A*, purified Nup157, which was analyzed by SDS-PAGE and Coomassie staining (*left*), was used for electron microscopy analysis. An overview electron micrograph of the negatively stained Nup157 (*middle*) and a gallery of selected particles of overexpressed or endogenous Nup157 (*right*) are shown. *B*, image processing of Nup157. Charge-coupled device image of Nup157 stained with 2% uranyl acetate. Different views of the surface representation of the three-dimensional map of Nup157 at ~17-Å resolution are shown. The threshold was chosen such that the volume accounted for 160 kDa. Different characteristic projections of Nup157 were derived from projection matching.

each other and which nucleoporins bridge between them. By reinvestigation of nucleoporin interactions, we identified several possible new Nup interactions and could reconstitute two of them *in vitro*. The observation that some of the interactions found *in vivo* were not reciprocal in the TAP purifications could be due to the possibility that a substoichiometric association does not always reveal a clear cut band on the SDS-polyacrylamide gel (please note that the TEV eluates from the various nucleoporin purifications were analyzed by SDS-PAGE and that only distinct bands discernible by Coomassie staining were excised and analyzed by MALDI-TOF mass spectrometry). The finding that only Nup120 was detected in the Nup157 preparation by mass spectrometry, but not the other subunits of the Nup84 complex, is not clear. However, Nup120 was found only as second hit in the peptide mass fingerprint analysis (see Fig. 1*D* and supplemental Fig. 2; the first hit was elongation factor eEF2, a possible contaminant) and, thus, its amount on the SDS-polyacrylamide gel cannot be estimated. Thus, we suspect that the other smaller subunits of the Nup84 complex were also present in purified Nup157, but because of a reduced Coomassie staining these subunits were not seen as distinct bands and therefore not analyzed by mass spectrometry.

Because of the observed substoichiometric interactions between Nup157, Nup145N, and the Nup84 complex, we performed *in vitro* reconstitution. In this way, we could reconstitute the interactions between nine nucleoporins, an assembly that represents 30% of all yeast nuclear pore proteins. However, the nine-subunit assembly, formed *in vitro* between the robust heptameric Nup84 and the dimeric Nup157-Nup145N complexes, is not stable enough for performing further biochemical purification. Thus, for a complete *in vitro* reconstitution of the NPC, low affinity interactions between NPC subcomplexes as described here could pose a problem. On the other hand, it is conceivable that several low affinity contacts as part of the entire NPC structure will stabilize the overall assembly.

We also wanted to analyze the structure of the Nup84 complex bound to Nup157 in the electron microscope. However, images of the Nup84 complex with bound Nup157 were not homogenous, and in only a few cases could contact between Nup157 molecules and the Y-shaped Nup84 complex be discerned.[6] We suspect that during specimen preparation for electron microscopy the unstable assembly of the Nup84 complex with Nup157 largely dissociated. Further work is required to reveal the structural details of how Nup157 is bound to Nup84 complexes.

Taking our biochemical data together, it is tempting to speculate that Nup157 (together with other structural Nups like Nup170) could link Nup84 complexes together, generating a higher structural assembly. A single Nup157 molecule, the structure of which resembles a clip with two spars, might

[6] M. Lutzmann, unpublished data.

access two separate Nup84 complexes. The Nup84 complex was estimated to occur in 16 copies per NPC and was suggested to represent a major part of the octagonal spoke-ring complex (2). However, other scenarios of interaction are also conceivable. Thus, the Nup157-Nup145N dimer could form a dual interface between two Nup84 complexes or Nup157 bridges between a Nup84 complex module and another structural Nup.

In addition to the *in vitro* reconstituted interactions of Nup157 and Nup145N with the Nup84 complex, we also describe in this work how Nup170 (homologue of Nup157), Mlp1, and Nic96 exhibit physical connections to the Nup84 complex. Because all of these nucleoporins except Nup145N lack FG repeat sequences, the identified contacts may be important for the structural organization of the NPC. The observation that Nic96 was found to be associated with purified Nup84 suggests that two key structural modules of the NPC, namely the stable Nic96 complex composed of Nic96, Nup57, Nup49, and Nsp1 (37) (see also Table I) and the Nup84 complex, could come in direct contact.

The *in vitro* finding that the Nup157-Nup145N heterodimer forms an assembly with the Nup84 complex, which can be easily dissociated, could reflect an *in vivo* requirement for a dynamic NPC biogenesis and/or organization. Notably, the conserved Nup145 is made as a precursor that is posttranslationally cleaved into two functionally separated domains, Nup145N and Nup145C in yeast (38, 39) or Nup98 and Nup96 in mammals (34, 40). The autoproteolytic cleavage of Nup145 is not essential in yeast but becomes essential in cells lacking Nup188 (38, 39). Moreover, self-cleavage of the Nup98-Nup96 precursor in mammals is crucial for NPC assembly (34, 40). Our work has revealed that both Nup145C and Nup145N have physical contact with the Nup84 complex, but the way these subunits interact with this NPC structural module is different. Whereas the Nup145C domain is a stable subunit of the Nup84 complex, the Nup145N domain is only loosely associated. It is possible that Nup145N has to be cleaved off from Nup145C to allow a dynamic interaction with the Nup84 complex.

Interesting in this context are recent studies showing that the binding dynamics between structural nucleoporins govern NPC permeability and affect channel gating (41). Notably, Goldfarb and colleagues observed that yeast cells lacking Nup170 exhibit a reversible dissociation of several structural nucleoporins (including members of the Nup84 complex) from NPCs upon the addition of aliphatic alcohols or chilling (41). Thus, dynamic rearrangements of structural NPC modules may be important not only for NPC assembly but also during translocation of large cargo through the transport channel, which may not be possible with a rigid NPC structure. Linker nucleoporins, which connect structural modules, could regulate this structural flexibility.

Finally, we report in this study the first structural analysis of a so-called large Nup (Nup157) that, like Nup188, is thought to be a structural constituent of the spoke-ring complex of the NPC (42–45). Isolation of this and other large Nups (*e.g.* Nup188 and Nup192) in *E. coli* was limited because of their low solubility. Thus, we developed a method to overexpress these large Nups in yeast followed by subsequent affinity purification and conventional chromatography. Because these three large Nups could be obtained in reasonable (microgram) amounts and pure form, we could perform the first biochemical and electron microscopy analyses (not shown in this study is the electron microscopy structure of Nup188 and Nup192).

The observation that Nup157 is not an elongated molecule but forms a hollow sphere is interesting in the structural context of the subunits of the Nup84 complex. Within the Nup84 complex, Nup120, Nup145C, and Nup85 exhibit elongated structures as shown by electron microscopy (15, 16). Notably, using computational and biochemical methods, several subunits of the yeast Nup84 complex (Nup120, Nup145C, and Nup85) and homologous vertebrate Nup107–160 complex were suggested to be elongated because they contain β-propeller/α-solenoid arrangements (46). Similarly, human Nup133 contains two domains, a carboxyl-terminal domain responsible for its interaction with its subcomplex through Nup107, and an amino-terminal domain whose crystal structure reveals a seven-bladed β-propeller (47). The N-terminal domain of Nup159 had been crystallized and was shown to contain an unusually asymmetric seven-bladed β-propeller (48). X-ray analysis of Nup157 or domains thereof should reveal which structural motifs occur in these large Nups.

Acknowledgments—We are grateful to Daniela Roser for technical assistance in TAP-tagging the yeast nucleoporins, Dr. Katja Strässer for the Nup60-TAP purification, Denise Lau for the high copy number ProtA-Nup192 plasmid, Sabine Merker and Petra Ihrig, under the supervision of Dr. J. Lechner (BZH, Heidelberg, Germany), for performing mass spectrometry, and Karsten Rippe (Kirchhoff-Institut für Physik, Heidelberg University) for help in analytical ultracentrifugation.

REFERENCES

1. Fahrenkrog, B., and Aebi, U. (2003) *Nat. Rev. Mol. Cell Biol.* **4,** 757–766
2. Suntharalingam, M., and Wente, S. R. (2003) *Dev. Cell* **4,** 775–789
3. Goldberg, M. W., and Allen, T. D. (1992) *J. Cell Biol.* **119,** 1429–1440
4. Ris, H. (1997) *Scanning* **19,** 368–375
5. Stoffler, D., Feja, B., Fahrenkrog, B., Walz, J., Typke, D., and Aebi, U. (2003) *J. Mol. Biol.* **328,** 119–130
6. Rout, M. P., Aitchison, J. D., Suprapto, A., Hjertaas, K., Zhao, Y., and Chait, B. T. (2000) *J. Cell Biol.* **148,** 635–651
7. Cronshaw, J. M., Krutchinsky, A. N., Zhang, W., Chait, B. T., and Matunis, M. J. (2002) *J. Cell Biol.* **158,** 915–927
8. Rexach, M., and Blobel, G. (1995) *Cell* **83,** 683–692
9. Bayliss, R., Littlewood, T., and Stewart, M. (2000) *Cell* **102,** 99–108
10. Fabre, E., and Hurt, E. (1997) *Annu. Rev. Genet.* **31,** 277–313
11. Rout, M. P., Aitchison, J. D., Magnasco, M. O., and Chait, B. T. (2003) *Trends Cell Biol.* **13,** 622–628
12. Ribbeck, K., and Görlich, D. (2001) *EMBO J.* **20,** 1320–1330
13. Ben-Efraim, I., and Gerace, L. (2001) *J. Cell Biol.* **152,** 411–417
14. Siniossoglou, S., Wimmer, C., Rieger, M., Doye, V., Tekotte, H., Weise, C., Emig, S., Segref, A., and Hurt, E. C. (1996) *Cell* **84,** 265–275
15. Siniossoglou, S., Lutzmann, M., Santos-Rosa, H., Leonard, K., Mueller, S., Aebi, U., and Hurt, E. C. (2000) in *J. Cell Biol.* **149,** 41–54
16. Lutzmann, M., Kunze, R., Buerer, A., Aebi, U., and Hurt, E. (2002) *EMBO J.* **21,** 387–397
17. Fontoura, B. M. A., Dales, S., Blobel, G., and Zhong, H. (2001) *Proc. Natl. Acad. Sci. U. S. A.* **98,** 3208–3213
18. Vasu, S., Shah, S., Orjalo, A., Park, M., Fischer, W. H., and Forbes, D. J. (2001) *J. Cell Biol.* **155,** 339–3354
19. Belgareh, N., Rabut, G., Bai, S. W., van Overbeek, M., Beaudouin, J., Daigle, N., Zatsepina, O. V., Pasteau, F., Labas, V., Fromont-Racine, M., Ellenberg, J., and Doye, V. (2001) *J. Cell Biol.* **154,** 1147–1160
20. Harel, A., Orjalo, A. V., Vincent, T., Lachish-Zalait, A., Vasu, S., Shah, S., Zimmerman, E., Elbaum, M., and Forbes, D. J. (2003) *Mol. Cell* **11,** 853–864
21. Walther, T. C., Alves, A., Pickersgill, H., Loiodice, I., Hetzer, M., Galy, V., Hulsmann, B. B., Kocher, T., Wilm, M., Allen, T., Mattaj, I. W., and Doye, V. (2003) *Cell* **113,** 195–206
22. Allen, N. P., Huang, L., Burlingame, A., and Rexach, M. F. (2001) *J. Biol. Chem.* **276,** 29268–29274
23. Santos-Rosa, H., Moreno, H., Simos, G., Segref, A., Fahrenkrog, B., Panté, N., and Hurt, E. (1998) *Mol. Cell. Biol.* **18,** 6826–6838
24. Hellmuth, K., Lau, D. M., Bischoff, F. R., Künzler, M., Hurt, E. C., and Simos, G. (1998) *Mol. Cell. Biol.* **18,** 6364–6386
25. Gavin, A.-C., Bösche, M., Krause, R., Grandi, P., Marzioch, M., Bauer, M., Schultz, J., Rick, J. M., Michon, A.-M., Cruciat, C. M., Remor, M., Höfert, C., Schelder, M., Brajenovic, M., Ruffner, H., Merino, A., Klein, K., Hudak, M., Dickson, D., Rudi, T., Gnau, V., Bauch, A., Bastuck, S., Huhse, B., Leutwein, C., Heurtier, M.-A., Copley, R. R., Edelmann, A., Querfurth, E., Rybin, V., Drewes, G., Raida, M., Bouwmeester, T., Bork, P., Seraphin, B., Kuster, B., Neubauer, G., and Superti-Furga, G. (2002) *Nature* **415,** 141–147
26. Rigaut, G., Shevchenko, A., Rutz, B., Wilm, M., Mann, M., and Séraphin, B. (1999) *Nat. Biotechnol.* **17,** 1030–1032
27. Bassler, J., Grandi, P., Gadal, O., Lessmann, T., Tollervey, D., Lechner, J., and Hurt, E. C. (2001) *Mol. Cell* **8,** 517–529
28. Crowther, R. A., Henderson, R., and Smith, J. M. (1996) *J. Struct. Biol.* **116,** 9–16
29. van Heel, M., Harauz, G., Orlova, E. V., Schmidt, R., and Schatz, M. (1996) *J. Struct. Biol.* **116,** 17–24
30. Huh, W. K., Falvo, J. V., Gerke, L. C., Carroll, A. S., Howson, R. W., Weissman, J. S., and O'Shea, E. K. (2003) *Nature* **425,** 686–691
31. Fischer, T., Strässer, K., Racz, A., Rodriguez-Navarro, S., Oppizzi, M., Ihrig, P., Lechner, J., and Hurt, E. (2002) *EMBO J.* **21,** 5843–5852

32. Nissan, T. A., Bassler, J., Petfalski, E., Tollervey, D., and Hurt, E. C. (2002) *EMBO J.* **21,** 5539–5547
33. Galy, V., Olivo-Martin, J., Scherthan, H., Doye, V., Rascalou, N., and Nehrbass, U. (2000) *Nature* **403,** 108–112
34. Fontoura, B. M. A., Blobel, G., and Matunis, M. J. (1999) *J. Cell Biol.* **144,** 1097–1112
35. Denning, D. P., Patel, S. S., Uversky, V., Fink, A. L., and Rexach, M. (2003) *Proc. Natl. Acad. Sci. U. S. A.* **100,** 2450–2455
36. Rout, M. P., and Aitchison, J. D. (2001) *J. Biol. Chem.* **276,** 16593–16596
37. Grandi, P., Doye, V., and Hurt, E. C. (1993) *EMBO J.* **12,** 3061–3071
38. Teixeira, M. T., Fabre, E., and Dujon, B. (1999) *J. Biol. Chem.* **274,** 32439–32444
39. Teixeira, M. T., Siniossoglou, S., Podtelejnikov, S., Bénichou, J.-C., Mann, M., Dujon, B., Hurt, E., and Fabre, E. (1997) *EMBO J.* **16,** 5086–5097
40. Rosenblum, J. S., and Blobel, G. (1999) *Proc. Natl. Acad. Sci. U. S. A.* **96,** 11370–11375
41. Shulga, N., Mosammaparast, N., Wozniak, R., and Goldfarb, D. S. (2000) *J. Cell Biol.* **149,** 1027–1038
42. Aitchison, J. D., Rout, M. P., Marelli, M., Blobel, G., and Wozniak, R. W. (1995) *J. Cell Biol.* **131,** 1133–1148
43. Kosova, B., Panté, N., Rollenhagen, C., and Hurt, E. (1999) *J. Biol. Chem.* **274,** 22646–22651
44. Zabel, U., Doye, V., Tekotte, H., Wepf, R., Grandi, P., and Hurt, E. C. (1996) *J. Cell Biol.* **133,** 1141–1152
45. Nehrbass, U., Rout, M. P., Maguire, S., Blobel, G., and Wozniak, R. W. (1996) *J. Cell Biol.* **133,** 1153–1162
46. Devos, D., Dokudovskaya, S., Alber, F., Williams, R., Chait, B. T., Sali, A., and Rout, M. P. (2004) *PLoS Biol.* **2,** e380
47. Berke, I. C., Boehmer, T., Blobel, G., and Schwartz, T. U. (2004) *J. Cell Biol.* **167,** 591–597
48. Weirich, C. S., Erzberger, J. P., Berger, J. M., and Weis, K. (2004) *Mol. Cell* **16,** 749–760

SUPPLEMENTAL FIGURES

Supplemental FIG. 1. *A*, Growth analyses of yeast strains expressing TAP-tagged nucleoporins. Wild-type haploid yeast strain and derived strains carrying the indicated TAP-tagged nucleoporin genes were analyzed by growth on YPD. Cells were spotted in 10^{-1} dilutions on YPD plates and it was grown for 2 days at 30°C or 3 days at 37°C.

Supplemental FIG. 2. Information on peptide mass fingerprinting for newly identified protein interactions. For a newly identified band (*identif. band*) in the indicated TAP-purification (*bait*), we show the hit number (*Hit-No.*), the *Probability Based Mowse Score* and the number of peptides, which were found for this band (*peptides found*). When the newly identified band was only found as second hit, also the first hit band and its MS data are given (in squared brackets).

Supplemental FIG. 3. Analytical sedimentation equilibrium ultracentrifugation of Nup145N. Absorbance scans at 280 nm recorded at 7000 rpm (curves 1, 3 and 5) and 10000 rpm (curves 2, 4 and 6) and at three different protein concentrations of 1.6 μM (curves 1 and 2), 3.2 μM (curves 3 and 4) and 7.4 μM (curves 5 and 6) are shown. The top panel displays the experimental data points and the fitted curve to a single component model with a molecular weight of 61.4 kDa. At the bottom the residuals of the fits are plotted.

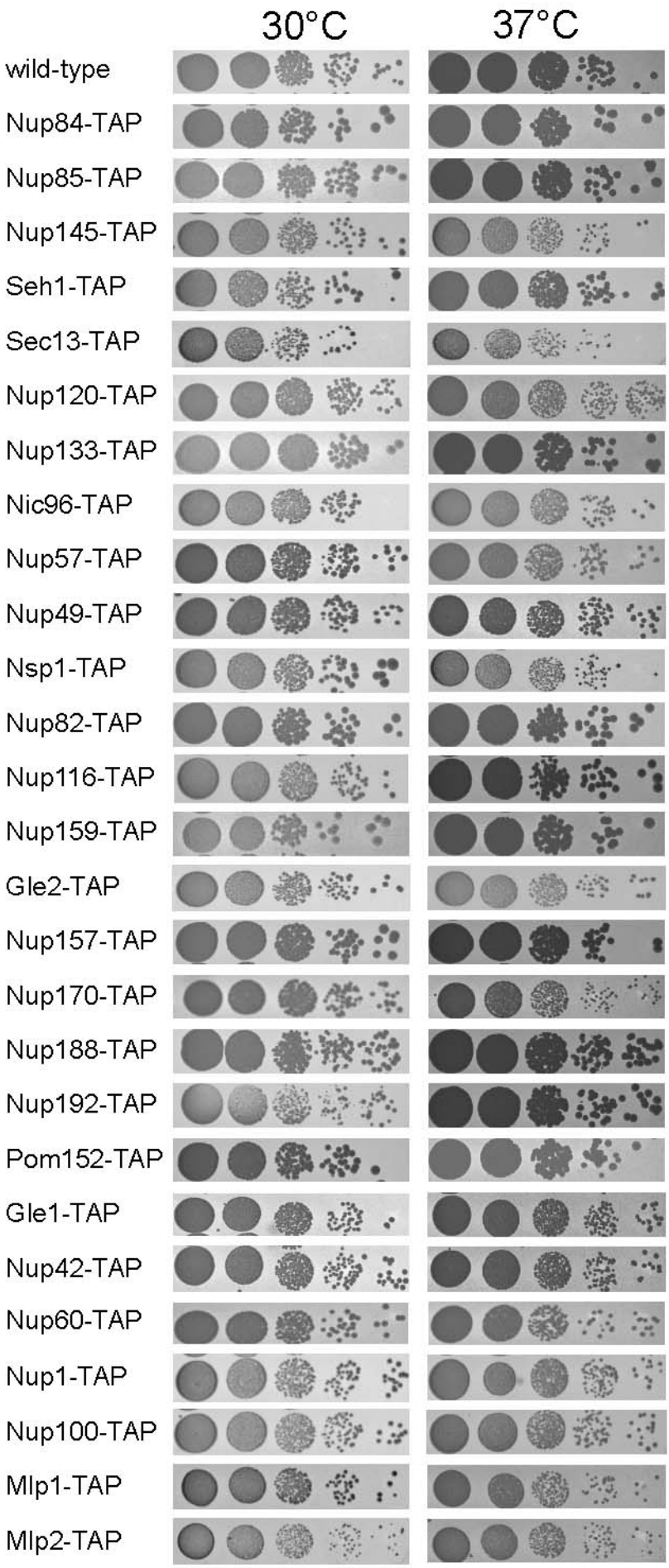

Supplemental Fig. 1 (Lutzmann et al., 2005)

Bait	*identif. Band*	*Hit-No.*	*Probability Based Mowse Score*	*Peptides found*
Gle2-TAP	Rea1-band	1	288	45
Nup116-TAP	Rea1-band	1	71	18
Nic96-TAP	Kap123-band	1	72	10
Nup145-TAP	Nup170-band	1	96	11
	Nup157-band	1	205	21
Nup84-TAP	Nup157-band	1	137	14
	Nup170-band	1	83	9
	Nup145N-band	1	53	7
	Mex67-band	1	88	9
	Nic96-band	2	61	7
	[Nup84	1	64	8]
Nup120-TAP	Nup157-band	1	92	12
	Nup170-band	2	33	5
	[Scp160	1	34	6]
	Nup145N-band	1	59	7
	Mlp1-band	1	42	12
Nup157-TAP	Nup120-band	2	60	12
	[eEF2	1	180	27]
	Nup145N-band	2	114	15
	[PABP	1	96	16]
Nup42-TAP	Gle1-band	1	247	25
Nup60-TAP	Sac3-band	1	71	12

Supplemental Fig. 2 (Lutzmann et al., 2005)

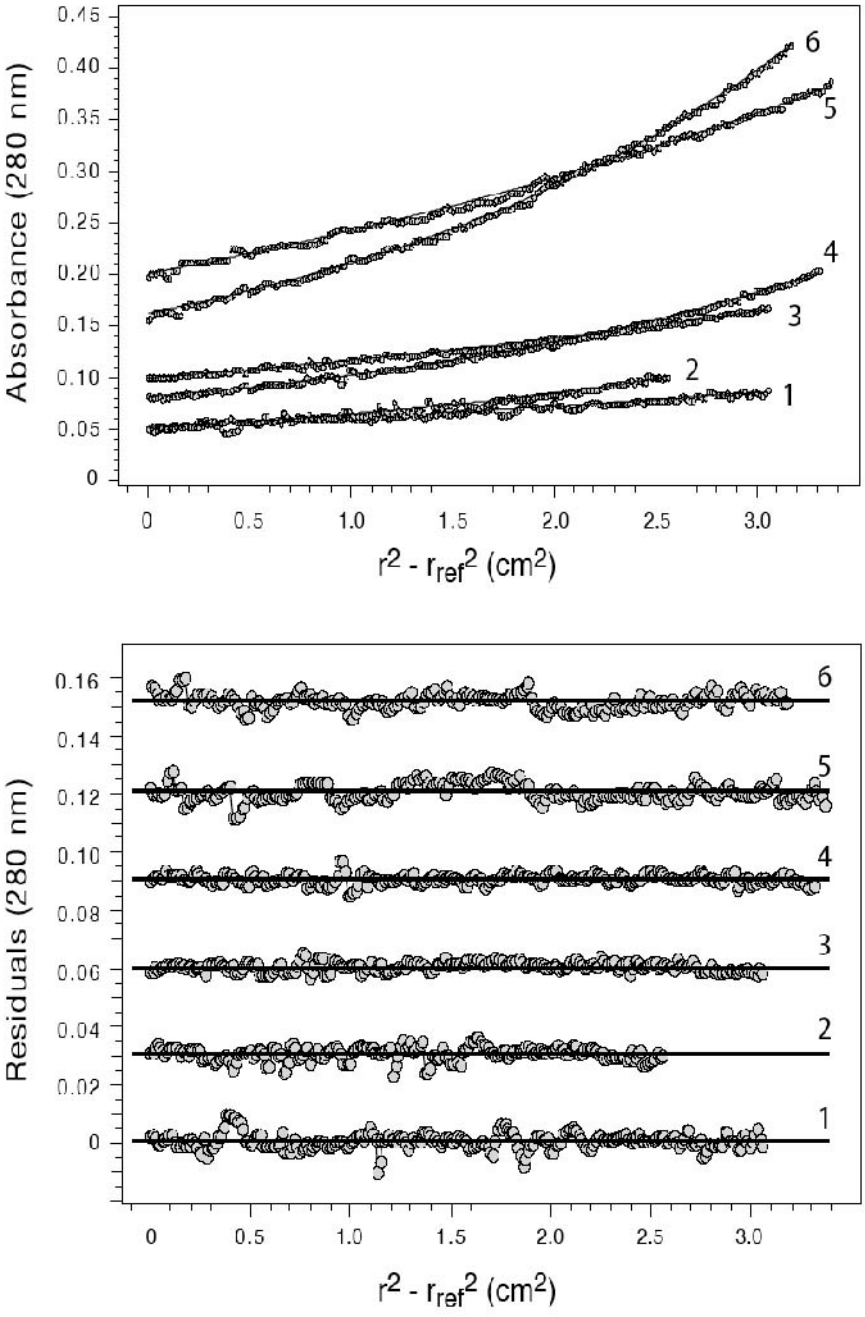

Supplemental Fig. 3 (Lutzmann et al., 2005)